

Polypyrrole-Fe₂O₃ nanocomposites with high dielectric constant: In Situ Chemical Polymerisation

**T. Bashir^{*a,d}, A. Shakoor^a, E.Ahmed^a, N. A. Niaz^a, Muhammad Saeed Akhtar^b,
Muhammad Rafi Raza^d, Mohammad Azad Malik^d and Peter J. S. Foot^e**

^aDepartment of Physics Bahauddin Zakariya University, Multan, 60800, Pakistan

^bDivision of Science and Technology, University of Education, College Road Township, Lahore, Pakistan

^cDepartment of Mechanical Engineering, COMSATS Institute of Information Technology, Sahiwal, Pakistan

^dSchool of Materials, The University of Manchester, Manchester, M13 9PL, UK

^eNanomaterials and Composites Research Group, Dept. of Chemical and Pharmaceutical Sciences, SEC Faculty, Kingston University London, KT1 2EE, UK.

***Corresponding author:** Tahir Bashir

E-mail: bashir_tahirphy@yahoo.com

Telephone Number: +92 300 7328006

SUMMARY

Novel nanocomposites of polypyrrole (PPy) dispersed with iron oxide (Fe_2O_3) particles have been synthesised by *in situ* chemical oxidative polymerisation of pyrrole in the presence of ammonium persulfate (APS) as an oxidising agent. The concentration of Fe_2O_3 was varied between 10-50wt% of PPy. The simultaneous polymerisation of pyrrole and oxide addition led to the complete synthesis of nanocomposites. A maximum dielectric constant of ~ 28500 was observed at 20wt% of Fe_2O_3 . The nanocomposites were characterised by X-ray diffraction (XRD), Fourier-transform infrared spectroscopy (FTIR), scanning electron microscopy (SEM) and transmission electron microscopy (TEM). XRD analysis confirmed the structure and crystallinity of the nanocomposites, and a strong interaction between PPy and Fe_2O_3 particles was observed by FTIR technique. SEM and TEM images showed that Fe_2O_3 particles had been coated with PPy by establishing a network during the polymerisation process. The values of dielectric constant were obtained from capacitance measurements. The value of dielectric constant for nanocomposites with 20wt% of Fe_2O_3 was observed to be almost 12 times that of the pure PPy matrix. The high value of dielectric constant indicated a high packing density of Fe_2O_3 particles in PPy matrix. These nanocomposites have potential applications in electronic or biomedical devices.

Keywords: Polypyrrole; Fe_2O_3 ; Nanocomposite; Dielectric constant; Polymerisation

1. INTRODUCTION

Research into conjugated polymers demonstrated that all polymers need not be insulators¹. These conjugated polymers have great scientific and technological significance due to their novel electrical, optical, electronic and optoelectronic characteristics^{2,3}. In the neutral state these materials demonstrate insulating or semiconducting characteristics^{4,5,6} and find applications in different fields like, solar cells^{7,8}, sensors⁹, organic light emitting diodes^{10,11} and opto-electronic devices¹².

Doping with metal oxides is one of the several ways to optimise the properties of these materials by carefully controlling the dopant into the polymer matrix¹³, resulting in new unique properties that cannot be achieved by single material^{14,15}. The inorganic materials due to their high surface to volume ratio are expected to alter the properties of organic polymer matrix rapidly. Above all, the main idea to synthesise these organic-inorganic networks is to obtain the unique composite materials demonstrating optimized properties between those of the organic and inorganic materials.

Among various polymers, polypyrrole (PPy) has reasonable thermal and environmental stability, significantly high electrical conductivity and simple route of synthesis^{16,17,18}. PPy has potential applications in electronic and electrochromic devices such as solar cells, super capacitors, energy storage^{19,20,21}, batteries, sensors^{22,23,24}, microwave absorption²⁵, antistatic coatings²⁶, charge storage²⁷, gas separation membranes²⁸ and capacitors²⁹. Its optical, electrical and mechanical properties can be improved by carefully doping of metal oxides in the PPy matrix^{30,31,32}.

However there is not much research done on the dielectric properties of PPy-Fe₂O₃ nanocomposites. Herein we report the synthesis of the organic-inorganic composites by chemical oxidative polymerisation with different iron oxide contents in the polymer. The effects of concentration of filler metal oxide have been studied by exploring their structural, morphological and dielectric characteristics in order to assess the applications of such nanocomposites for electronic and related fields.

2. EXPERIMENTAL

2.1 Materials

All the chemicals were purchased from reputable companies. Pyrrole (analytical grade, 99%) was purchased from Sigma-Aldrich, stored at 5°C and vacuum distilled prior to use. APS and Fe₂O₃ were supplied by Merck. All other supplementary chemicals and solvents such as acetone, hydrochloric acid (HCl), chloroform and methanol were obtained from Fluka and used as received. Ultrapure deionised water (Seralpur delta) was used during all synthesis procedures.

2.2 Synthesis of PPy and PPy-Fe₂O₃ nanocomposites

The chemical oxidative polymerisation method was carried out for the synthesis of PPy and PPy-Fe₂O₃ nanocomposites as described earlier³³. Vacuum distilled pyrrole (10 g) and ammonium persulfate (APS) (12.25 g) were dissolved separately in deionised water for synthesis of PPy-Fe₂O₃ nanocomposites. The pyrrole mixture was acidified gradually by dropwise addition of HCl (5 mL). At the next stage, 10wt% Fe₂O₃ (1 g) ultrasonically dispersed in deionised water was added to the pyrrole solution and the mixture was well stirred for 3 h. Afterwards, the solution of APS was added dropwise by dropping funnel into the mixture containing pyrrole, HCl and Fe₂O₃ under vigorous stirring. Same synthesis procedure was adopted for other concentrations of Fe₂O₃ *i.e.*, 20, 30, 40 and 50 wt%. The prepared nanocomposites were designated as P-1, P-2, P-3, P-4 and P-5 respectively. The suspension of obtained composites left overnight in fume hood. After ensuring the complete polymerisation, the suspensions were successively filtered and washed with deionised water. The precipitate was then dried under vacuum at 70°C for 24 h. To achieve complete homogeneity of the constituents, the dried precipitates were well crushed and ground for 1 hour by an A-grade mortar and pestle, cleaned with acetone and deionised water. Pellets of the ground powder were prepared using a hydraulic press with a pressure of 30 kN applied for 2 min before further characterisation.

The powder X-ray diffraction patterns of samples were obtained by using an automated diffractometer, Bruker-AXS D8, using Cu K α radiation. The operating voltage and current of the machine were maintained at 40 kV and 30 mA respectively. The samples were mounted on standard holders and diffraction spectra were recorded over the range of 10-60 degrees (2-theta) with a counting time of 3 s and step size 0.10 degree. Molecular structure was analysed through FTIR spectra recorded by Perkin Elmer FTIR spectrometer in the range from 500 to 3500 cm⁻¹. The surface morphology of nanocomposites was observed by an EVO50 ZEISS scanning electron microscope and a Philips CM 12 transmission electron microscope respectively. For the

measurement of dielectric properties a Wayne Kerr LCR meter Model 4275 was used in the frequency range from 20 Hz to 20 MHz. The obtained data were transformed into dielectric constants by applying the relation:

$$C = \frac{\epsilon_r \epsilon_0 A}{d} \quad (1)$$

where ϵ_r is relative permittivity, C is capacitance, ϵ_0 is permittivity of free space, d and A are thickness and cross sectional area of the pellets respectively. The thickness and diameter of the samples were measured by a digital micrometer.

3. RESULTS AND DISCUSSION

3.1 X-ray Diffraction (XRD)

XRD patterns reveal that pure PPy is amorphous³⁴ and PPy-Fe₂O₃ nanocomposites are polycrystalline in nature due to the existence of crystalline material *i.e.*, Fe₂O₃ whose diffraction pattern is shown in Figure 1. The diffraction patterns of pure PPy along with its nanocomposites are depicted in Figure 2. An increase in the intensity of diffraction peaks is observed with increasing concentration of Fe₂O₃ in the nanocomposites. For pure PPy, the existence of a broader peak at 2θ between 20-28° has already been reported, and corresponds to the characteristic peak of pure PPy³⁵. The appearance of this broad peak in all nanocomposites confirms the existence of PPy, and its intensity decreases with an increase in Fe₂O₃ content. Figures 2(a-f) show diffraction peaks corresponding to the (102), (104), (110), (113), (024) and (116) planes of Fe₂O₃ at 24.51, 33.28, 35.669, 40.880, 49.495 and 54.14 degrees 2θ respectively. The observed diffraction peaks are well matched with the JCPDS data Card No. 13-534.

The variation in crystallite size of the nanocomposites as a function of Fe₂O₃ concentration was estimated by means of the Scherrer relation:

$$d = \frac{k\lambda}{\beta \cos\theta} \quad (2)$$

Here d is crystallite size for individual peak, k is the unit cell geometry dependent constant, whose value is typically between 0.85 to 0.99, λ is the wavelength of incident X-ray, β is the line broadening at full width at half maximum (FWHM) of the individual peaks and θ is the

Bragg angle. For crystallite size measurement, the strongest peak corresponding to the (104) plane was selected. The average value of crystallites observed to be in the range from 18 to 36 nm. A slight shift in diffraction angle of the (104) diffraction peak is observed for all nanocomposites with respect to the Fe_2O_3 pattern as reported earlier³⁶. The structural parameters for nanocomposites are listed in Table 1.

3.2 Fourier Transform Infrared Spectroscopy (FTIR)

Figure 3 depicts the FTIR spectra correlating the chemical structure of PPy and PPy- Fe_2O_3 nanocomposites. For pure PPy, FTIR spectrum is in close agreement with one reported earlier³⁷. The spectral bands observed at 780, 1090 and 1160 cm^{-1} are due to C-H out-of-plane ring deformation, C-H/N-H in-plane deformation modes and C-H interplane bending respectively³⁸. The spectral bands at 1428 and 1550 cm^{-1} are associated with CH_3 absorption and interacting C-C vibrations respectively³⁹. The spectral bands located at 1490 and 1728 cm^{-1} exhibit C=C vibrations of the quinoid rings^{40,41}. It is noticeable that peak positions of all PPy- Fe_2O_3 nanocomposites are displaced towards higher wavenumbers than those observed in pure PPy. This displacement is likely to result from the process of active electronic interaction between PPy and Fe_2O_3 particles⁴². The inclusion of Fe_2O_3 causes the creation of hydrogen bonds between the NH protons and oxygen atoms on the Fe_2O_3 . As a result N-H bond and the stretching intensity become weaker^{43,44}.

3.3 Scanning Electron Microscopy (SEM)

Figure 4 (a) shows SEM images of PPy representing the formation of a porous spongy irregular agglomerated structure. Figures 4(b) to 4(f) depict the SEM images of PPy- Fe_2O_3 nanocomposites, showing an enhancement in the attachment of Fe_2O_3 particles to the polymer matrix, with an increase in Fe_2O_3 concentration. It is clearly visible from the micrographs that Fe_2O_3 particles (white colour) were embedded almost completely in the PPy matrix, confirming the formation of nanocomposites. Furthermore, the presence of Fe_2O_3 particles covered by PPy chain agglomerates and the resulting microstructure shows the presence of modified aggregated porous regions which would facilitate good electrical conductivity and dielectric response.

3.4 Transmission Electron Microscopy (TEM)

For detailed surface characterisation of PPy-Fe₂O₃ nanocomposites, transmission electron microscopy of selected samples was carried out. The morphology shown from Figures 5(a) to 5(c) reveals the presence of two distinct regions, *i.e.* a black core of iron oxide particles well wrapped by outer grey shells of PPy with an average diameter ranging from 30 to 36 nm. This observation is evidence for successful polymerisation of polymer-metal oxide nanocomposites. The increment in Fe₂O₃ concentration seems helpful for it to occupy the porous sites of the polymer, which could result in improvement of various structural, electrical and magnetic properties.

3.5 Dielectric Constant measurements

The dielectric constant (ϵ') of a material refers to its capacity to store energy in the presence of an electric field, while the dielectric loss (ϵ'') expresses a concomitant loss or dissipation of energy^{45,46}. Under the influence of an applied electric field, a conductive material always experiences the induction of two types of currents: (i) displacement current and (ii) conduction current⁴⁷. The former type of current arises from localised bound charges, responsible for electronic, ionic, orientational and space charge polarisation (ϵ') within the material. The latter type is typically induced due to mobile charges and is responsible for dielectric losses (ϵ'') within the material⁴⁸.

In composite materials, heterogeneity of organic and inorganic material would result in the domination of space charge polarisation, whereas in conjugated polymer system, polarons and/or bipolarons are mobile and free to hop between different sites along the polymer chain. The space charge polarisation arises from the restricted mobility of bound carrier dipoles, which leads to a form of orientational polarisation⁴⁹, responsible for a decreasing value of ϵ' with an increase in frequency. Figure 6 shows the graph of ϵ' vs. frequency for pure PPy and PPy-Fe₂O₃ nanocomposites. A sharp decrease in the value of ϵ' is observed initially from 20 Hz to 1 kHz that would be well explained on the basis of space charge effects⁵⁰ and interfacial polarisation⁵¹. During that process the charge carriers appearing from the Maxwell-Wagner-Sillars polarisation effect, are stored at the interfaces of the constituents. These interfaces could be either inner dielectric boundaries or external sample-electrode contacts⁵².

After 1 kHz, the sharp decrease in ϵ' slowed down and became linear presented no further reasonable change in higher frequency regions. The decrease in ϵ' at higher frequency region is due to the dielectric relaxation response of the material⁵³. The dielectric relaxation usually occurs due to delayed molecular polarisation within the external applied field⁵⁴. P-2 nanocomposite exhibits the highest values of ϵ' among all the samples, which might be due to the strong interaction between PPy and Fe₂O₃ particles⁵⁵. The obtained ϵ' values of PPy are 2408 and 371 at 20 Hz and 1 kHz respectively, whereas for the case of P-2 nanocomposite higher values of dielectric constant are obtained *i.e.*, 28500 and 4169 at 20 Hz and 1 kHz respectively. For the higher frequency regions ϵ' remained persistent, because induced moments could no longer synchronise themselves with the applied field in that frequency range. The dependence of ϵ' on concentration of Fe₂O₃ is shown in Figure 6 (inset), presenting the highest value of ϵ' for P-2 nanocomposite.

3.6 Dielectric Loss Measurements

Dielectric loss (ϵ'') response to frequency in PPy and PPy-Fe₂O₃ nanocomposites is shown in Figure 7. The observed energy loss is due to the existence of moving dipoles between polymer and the metal oxide. These moving dipoles are a result of the strong interactions between the constituents. Since the existence of moving dipoles is less in nanocomposites as compared to PPy, that is the reason for increased value of dielectric loss in nanocomposites as compared to PPy and is confirmed experimentally. Dielectric loss varies with the particle size of the nanocomposites and is usually high for large particles⁵⁶. The inset of Figure 7 displays the highest value of ϵ'' for P-2 nanocomposite.

The values of ϵ'' for PPy are 6032 and 361 at 20 Hz and 1 kHz respectively, whereas in the case of P-2 nanocomposite these values are 278472 and 26315 at 20 Hz and 1 kHz respectively. The observed values of ϵ' and ϵ'' for all the samples are listed in Table 2.

The ratio of ϵ'' to ϵ' is a measure of energy dissipation of a material, denoted as “ $\tan \delta$ ” provides the basic information about an efficient energy absorbing material. The dependence of $\tan \delta$ on frequency for PPy and PPy-Fe₂O₃ nanocomposites is presented in Figure 8. A decreasing trend in the value of $\tan \delta$ is observed with gradual increase in frequency. The highest value of $\tan \delta$ of each sample was found to be different depending on the loading of Fe₂O₃ content and it was

found to reach a maximum at 20wt% Fe₂O₃ concentration. Those nanocomposites demonstrating high dielectric constant values in low frequency regions are suitable candidates for use in charge storing devices, electro-magnetic interference (EMI) shielding and decoupling capacitor applications⁵⁷.

4. CONCLUSION

PPy-Fe₂O₃ nanocomposites have been prepared by incorporation of Fe₂O₃ particles into a PPy matrix. A uniform dispersion of the Fe₂O₃ particles and strong interaction between the PPy and the Fe₂O₃ particles have been observed by XRD and FTIR respectively. An increasing trend of the dielectric constant up to 20wt% and then a gradual decrease up to 50wt% of Fe₂O₃, has been observed, with a maximum almost 12 times that of pure PPy. The surface morphology clearly reveals the presence of evenly-dispersed Fe₂O₃ particles in the PPy matrix, in accordance with their proportion and the successful formation of nanocomposites. The synthesised nanocomposites could be helpful in applications such as fabricating charge storing devices, electromagnetic interference (EMI) shielding and decoupling capacitor applications.

ACKNOWLEDGEMENT

The authors would like to acknowledge the Higher Education Commission (HEC) of Pakistan for their financial support under International Research Support Initiative Program (IRSIP) vide letter number 1- 8/HEC/HRD/2015/4026.

CONFLICTS OF INTEREST

The authors declare that they have no conflict of interest.

REFERENCES

1. Huang J. Syntheses and applications of conducting polymer polyaniline nanofibers. *Pure and Applied Chemistry* **78** (2006) 15-27.
2. Brabec CJ, Sariciftci NS, Hummelen JC. Plastic solar cells. *Advanced Functional Materials* **11** (2001) 15-26.
3. Reynolds JR, Skotheim TA, Elsenbaumer RL. *Handbook of Conducting Polymers*. Marcel Dekker (1998).
4. Bashir T, Shakoor A, Ahmad E, Saeed M, Niaz N, et al. Structural, morphological, and electrical properties of polyaniline-Fe₂O₃ nanocomposites. *Polymer Science Series B* **57** (2015) 257-263.
5. Mane AT, Navale ST, Sen S, Aswal DK, Gupta SK, et al. Nitrogen dioxide (NO₂) sensing performance of p-polypyrrole/n-tungsten oxide hybrid nanocomposites at room temperature. *Organic Electronics* **16** (2015) 195-204.
6. MacDiarmid AG. "Synthetic metals": A novel role for organic polymers (Nobel lecture). *Angewandte Chemie International Edition* **40** (2001) 2581-2590.
7. Lee JK, Kim WS, Lee HJ, Shin WS, Jin SH, et al. Preparations and photovoltaic properties of dye - sensitized solar cells using thiophene - based copolymers as polymer electrolytes. *Polymers for Advanced Technologies* **17** (2006) 709-714.
8. Chang YM, Su WF, Wang L. Photoactive polythiophene: titania hybrids with excellent miscibility for use in polymer photovoltaic cells. *Macromolecular Rapid Communications* **29** (2008) 1303-1308.
9. Yoon H, Chang M, Jang J. Formation of 1D poly(3,4 - ethylenedioxythiophene) nanomaterials in reverse microemulsions and their application to chemical sensors. *Advanced Functional Materials* **17** (2007) 431-436.
10. Dobbertin T, Werner O, Meyer J, Kammoun A, Schneider D, et al. Inverted hybrid organic light-emitting device with polyethylene dioxythiophene-polystyrene sulfonate as an anode buffer layer. *Applied Physics Letters* **83** (2003) 5071-5073.
11. Fehse K, Schwartz G, Walzer K, Leo K. Combination of a polyaniline anode and doped charge transport layers for high-efficiency organic light emitting diodes. *Journal of Applied Physics* **101** (2007) 124509.

12. Genies E, Lapkowski M. Application of electronic conducting polymers as sensors: PANI in the solid state for detection of biological ions in solutions. *Synthetic Metals* **28** (1989) 769-773.
13. Mallikarjuna N, Manohar S, Kulkarni P, Venkataraman A, Aminabhavi T. Novel high dielectric constant nanocomposites of polyaniline dispersed with γ - Fe₂O₃ nanoparticles. *Journal of Applied Polymer Science* **97** (2005) 1868-1874.
14. Tong X, Zhao H, Tang T, Feng Z, Huang B. Preparation and characterization of poly (ethyl acrylate)/bentonite nanocomposites by in situ emulsion polymerization. *Journal of Polymer Science Part A: Polymer Chemistry* **40** (2002) 1706-1711.
15. Lim S, Kim J, Chin I, Kwon Y, Choi H. Preparation and interaction characteristics of organically modified montmorillonite nanocomposite with miscible polymer blend of poly(ethylene oxide) and poly(methyl methacrylate). *Chemistry of Materials* **14** (2002) 1989-1994.
16. Münstedt H. Ageing of electrically conducting organic materials. *Polymer* **29** (1988) 296-302.
17. Skotheim TA, Reynolds J. *Conjugated polymers: theory, synthesis, properties, and characterisation*. CRC press (2006).
18. Armes SP. Optimum reaction conditions for the polymerisation of pyrrole by iron (III) chloride in aqueous solution. *Synthetic Metals* **20** (1987) 365-371.
19. Zhang J, Kong L-B, Li H, Luo Y-C, Kang L. Synthesis of polypyrrole film by pulse galvanostatic method and its application as supercapacitor electrode materials. *Journal of Materials Science* **45** (2010) 1947-1954.
20. Keothongkham K, Pimanpang S, Maiaugree W, Saekow S, Jareenboon W, et al. Electrochemically deposited polypyrrole for dye-sensitised solar cell counter electrodes. *International Journal of Photoenergy* (2012) 2012.
21. Olsson H, Carlsson DO, Nyström G, Sjödin M, Nyholm L, et al. Influence of the cellulose substrate on the electrochemical properties of paper-based polypyrrole electrode materials. *Journal of Materials Science* **47** (2012) 5317-5325.
22. Xia J, Chen L, Yanagida S. Application of polypyrrole as a counter electrode for a dye-sensitised solar cell. *Journal of Materials Chemistry* **21** (2011) 4644-4649.

23. Montoya P, Mejía S, Goncales VR, de Torresi SIC, Calderón JA. Performance improvement of macroporous polypyrrole sensor for detection of ammonia by incorporation of magnetite nanoparticles. *Sensors and Actuators B: Chemical* **213** (2015) 444-451.
24. Ke R, Zhang X, Wang L, Zhang C, Zhang S, et al. Electrochemiluminescence sensor based on graphene oxide/polypyrrole/CdSe nanocomposites. *Journal of Alloys and Compounds* **622** (2015) 1027-1032.
25. Jiang W, Sun M, Zhang K, Wu F, Xie A, et al. Three-dimensional (3D) α -Fe₂O₃/polypyrrole (PPy) nanocomposite for effective electromagnetic absorption. *AIP Advances* **6** (2016) 065021.
26. Entezami AA, Massoumi B. Artificial muscles, biosensors and drug delivery systems based on conducting polymers: a review. *Iranian Polymer Journal* **15** (2006) 13-30.
27. Mallouki M, Tran-Van F, Sarrazin C, Chevrot C, Fauvarque J. Electrochemical storage of polypyrrole-Fe₂O₃ nanocomposites in ionic liquids. *Electrochimica Acta* **54** (2009) 2992-2997.
28. Hosseini SH, Entezami AA. Studies of thermal and electrical conductivity behaviours of polyaniline and polypyrrole blends with polyvinyl acetate, polystyrene and polyvinyl chloride. *Iranian Polymer Journal* **14** (2005) 201-209.
29. Krings L, Havinga E, Donkers J, Vork F. The application of polypyrrole as counterelectrode in electrolytic capacitors. *Synthetic Metals* **54** (1993) 453-460.
30. Srivastava V, Maydannik P, Sillanpää M. Synthesis and characterization of PPy@ NiO nanoparticles and their use as adsorbent for the removal of Sr (II) from aqueous solutions. *Journal of Molecular Liquids* **223** (2016) 395-406.
31. Liu Y, Ma H, Zhang Y, Pang X, Fan D, et al. Visible light photoelectrochemical aptasensor for adenosine detection based on CdS/PPy/gC₃N₄ nanocomposites. *Biosensors and Bioelectronics* **86** (2016) 439-445.
32. Ghaemi N, Daraei P. Enhancement in copper ion removal by PPy@ Al₂O₃ polymeric nanocomposite membrane. *Journal of Industrial and Engineering Chemistry* **40** (2016) 26-33.
33. Khan A, Farooq M. Giant dielectric constant and low loss tangent in polypyrrole doped with dodecylbenzene sulfonic acid. *Polymer Science--Series A* (2013) 55.

34. Kassim A, Davis F, Mitchell G. The role of the counter-ion during electropolymerisation of polypyrrole-camphorsulfonate films. *Synthetic Metals* **62** (1994) 41-47.
35. Kassim A, Mahmud HE, Yee LM, Hanipah N. Electrochemical preparation and characterization of polypyrrole-polyethylene glycol conducting polymer composite films. *Pacific Journal of Science & Technology* **7** (2006) 103-107.
36. Murugendrappa M, Khasim S, Prasad MA. Synthesis, characterization and conductivity studies of polypyrrole-fly ash composites. *Bulletin of Materials Science* **28** (2005) 565-569.
37. Chougule MA, Pawar SG, Godse PR, et al. Synthesis and characterization of polypyrrole (PPy) thin films. *Soft Nanoscience Letters* **1** (2011) Article ID:3660, DOI:10.4236/snl.2011.11002.
38. Li X, Wan M, Wei Y, Shen J, Chen Z. Electromagnetic functionalized and core-shell micro/nanostructured polypyrrole composites. *The Journal of Physical Chemistry B* **110** (2006) 14623-14626.
39. Yuvaraj H, Woo MH, Park EJ, Jeong YT, Lim KT. Polypyrrole/ γ -Fe₂O₃ magnetic nanocomposites synthesized in supercritical fluid. *European Polymer Journal* **44** (2008) 637-644.
40. Neetika G, Kumar D, Tomar S. Thermal behaviour of chemically synthesized polyanilines/polystyrene sulphonic acid composites. *International Journal of Materials and Chemistry* **2** (2012) 79-85.
41. Xiaotun Y, Lingge X, Choon NS, Hardy CSO. Magnetic and electrical properties of polypyrrole-coated γ -Fe₂O₃ nanocomposite particles. *Nanotechnology* **14** (2003) 624.
42. Bandgar DK, Navale ST, Vanalkar SA, Kim JH, Harale NS, et al. Synthesis, structural, morphological, compositional and electrical transport properties of polyaniline/ α -Fe₂O₃ hybrid nanocomposites. *Synthetic Metals* **195** (2014) 350-358.
43. Xia H, Wang Q. Ultrasonic irradiation: a novel approach to prepare conductive polyaniline/nanocrystalline titanium oxide composites. *Chemistry of Materials* **14** (2002) 2158-2165.
44. Kowsari E, Faraghi G. Ultrasound and ionic-liquid-assisted synthesis and characterization of polyaniline/Y₂O₃ nanocomposite with controlled conductivity. *Ultrasonics Sonochemistry* **17** (2010) 718-725.

45. Li Y, Chen G, Li Q, Qiu G, Liu X. Facile synthesis, magnetic and microwave absorption properties of Fe₃O₄/polypyrrole core/shell nanocomposite. *Journal of Alloys and Compounds* **509** (2011) 4104-4107.
46. Cui C, Du Y, Li T, Zheng X, Wang X, et al. Synthesis of electromagnetic functionalized Fe₃O₄ microspheres/polyaniline composites by two-step oxidative polymerization. *The Journal of Physical Chemistry B* **116** (2012) 9523-9531.
47. Dhawan S, Ohlan A, Singh K. Designing of nano composites of conducting polymers for EMI shielding. INTECH Open Access Publisher (2011).
48. Gandhi N, Singh K, Ohlan A, Singh D, Dhawan S. Thermal, dielectric and microwave absorption properties of polyaniline–CoFe₂O₄ nanocomposites. *Composites Science and Technology* **71** (2011) 1754-1760.
49. Ohlan A, Singh K, Chandra A, Singh V, Dhawan S. Conjugated polymer nanocomposites: synthesis, dielectric, and microwave absorption studies. *Journal of Applied Physics* **106** (2009) 044305-044301.
50. Farid M, Ahmad I, Aman S, Kanwal M, Murtaza G, et al. Structural, electrical and dielectric behavior of Ni_xCo_{1-x}Nd_yFe_{2-y}O₄ nano-ferrites synthesized by sol-gel method. *Digest Journal of Nanomaterials and Biostructures* **10** (2015) 265-275.
51. Zhu J, Zhang X, Haldolaarachchige N, Wang Q, Luo Z, et al. Polypyrrole metacomposites with different carbon nanostructures. *Journal of Materials Chemistry* **22** (2012) 4996-5005.
52. Kremer F, Schönhals A. *Broadband Dielectric Measurement Techniques* (10⁻⁶ Hz to 10¹² Hz). Springer (2012).
53. Zhu J, Gu H, Luo Z, Haldolaarachchige N, Young DP, et al. Carbon nanostructure-derived polyaniline metacomposites: electrical, dielectric, and giant magnetoresistive properties. *Langmuir* **28** (2012) 10246-10255.
54. Rosenbaum R, Milner A, Haberkern R, Häussler P, Palm E, et al. Magnetoresistance of an insulating quasicrystalline AlPdRe film in large magnetic fields. *Journal of Physics: Condensed Matter* **13** (2001) 3169.
55. Sun Z-X, Su F-W, Forsling W, Samskog P-O. Surface characteristics of magnetite in aqueous suspension. *Journal of Colloid and Interface Science* **197** (1998) 151-159.

56. Kharabe R, Devan R, Kanamadi C, Chougule B. Dielectric properties of mixed Li-Ni-Cd ferrites. *Smart Materials and Structures* **15** (2006) N36.
57. Panwar V, Mehra R. Study of electrical and dielectric properties of styrene-acrylonitrile/graphite sheets composites. *European Polymer Journal* **44** (2008) 2367-2375.

Figure Captions

Fig 1: XRD pattern of Fe_2O_3

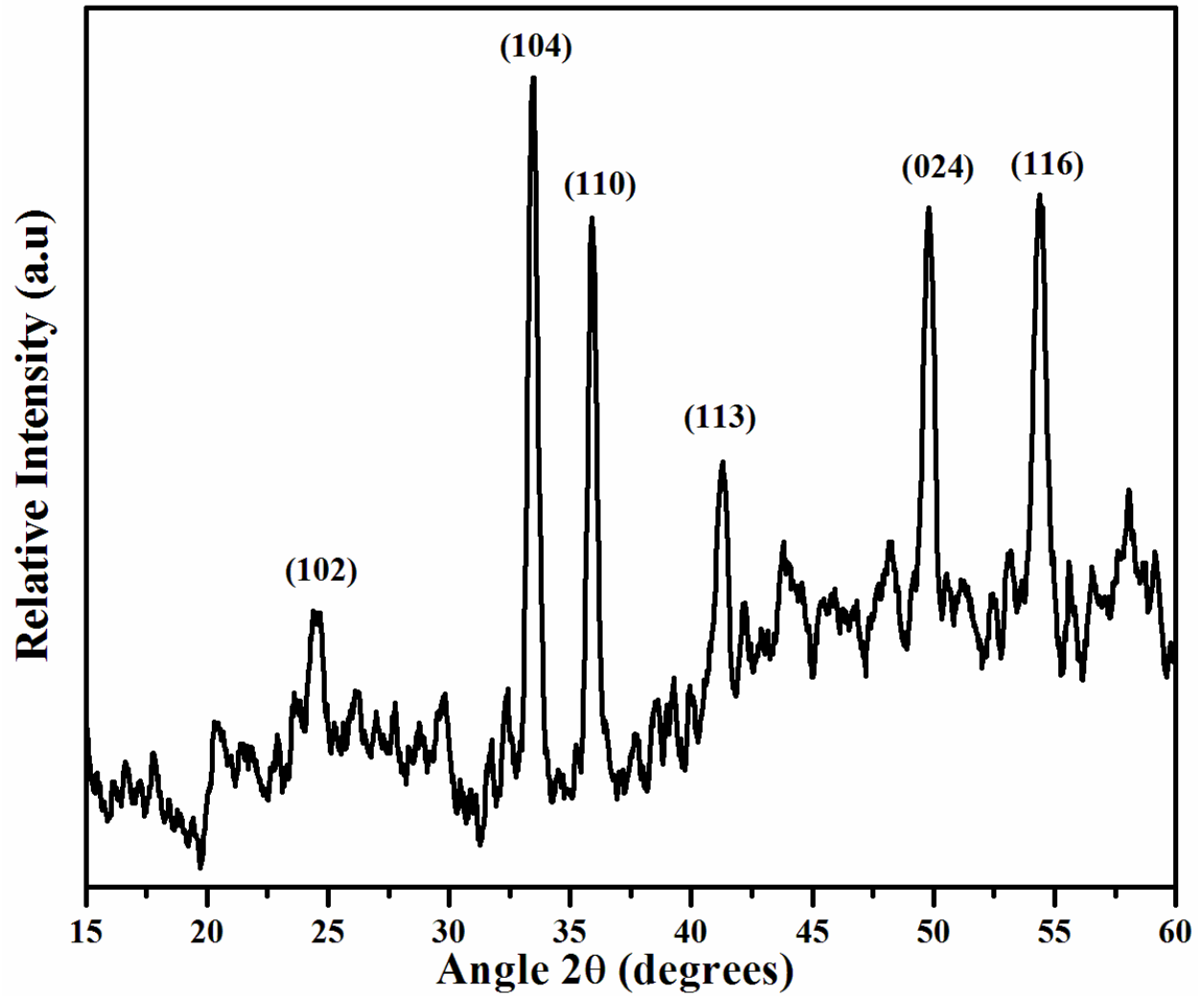


Fig 2: XRD patterns of (a) PPy (b) P-1 (c) P-2 (d) P-3 (e) P-4 (f) P-5

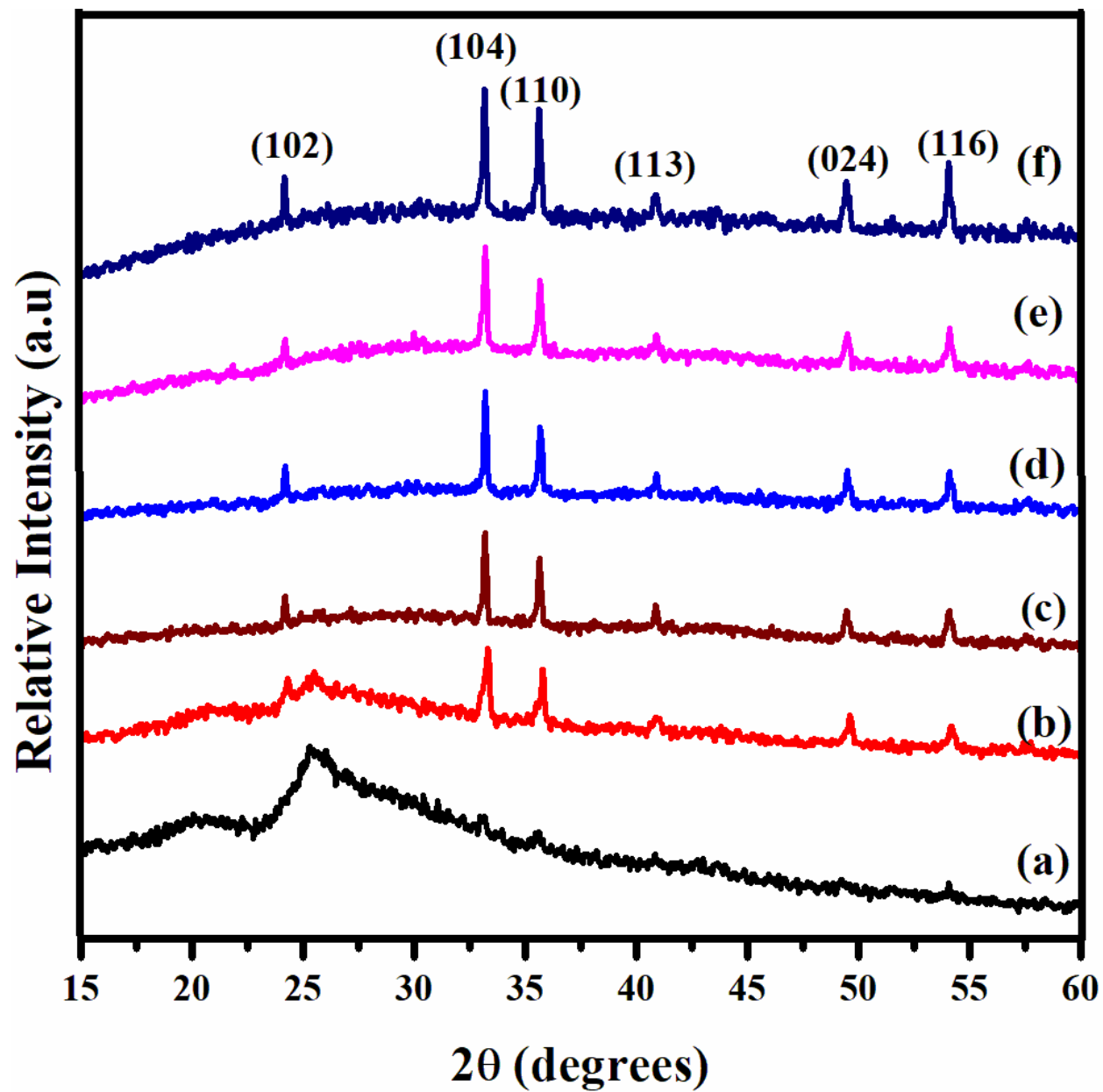


Fig 3: FTIR spectra of (a) PPy (b) P-1 (c) P-2(d) P-3 (e) P-4 (f) P-5

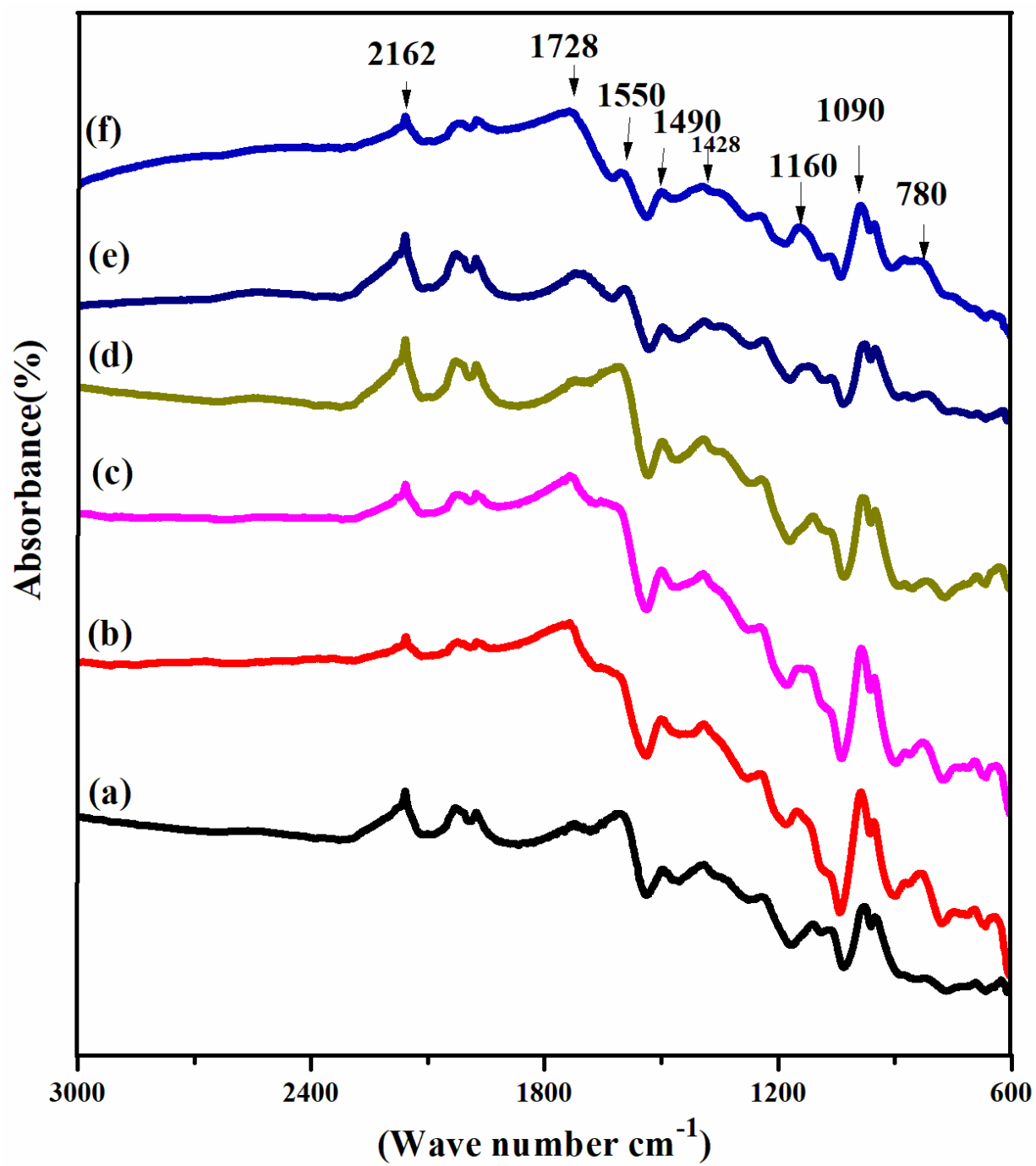


Fig 4 (a): SEM image of PPy

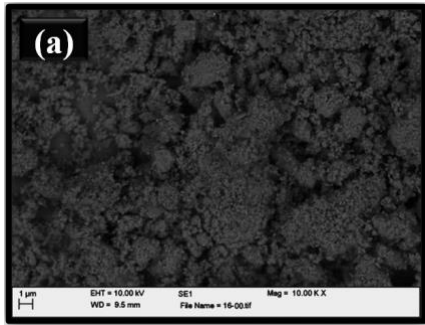


Fig 4 (b): SEM image of P-1

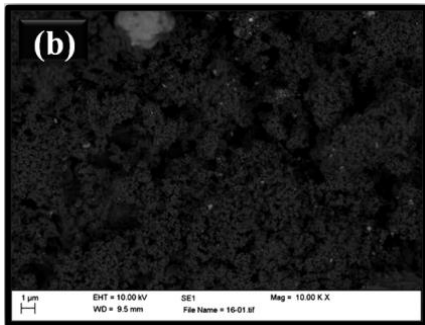


Fig 4 (c): SEM image of P-2

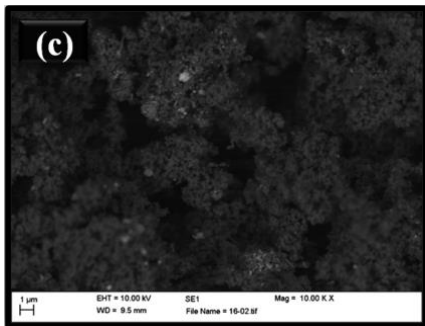


Fig 4 (d): SEM image of P-3

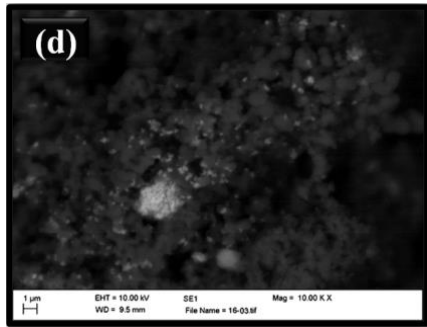


Fig 4 (e): SEM image of P-4

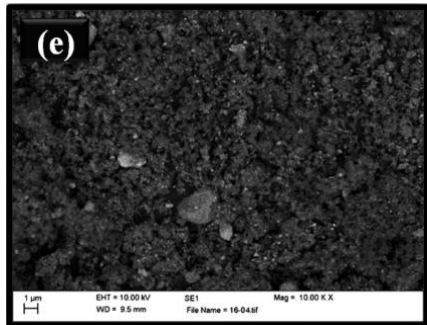


Fig 4 (f): SEM image of P-5

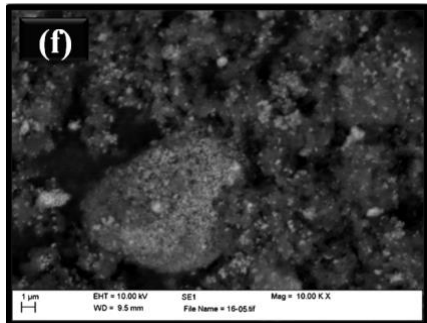


Fig 5 (a): TEM image of P-1

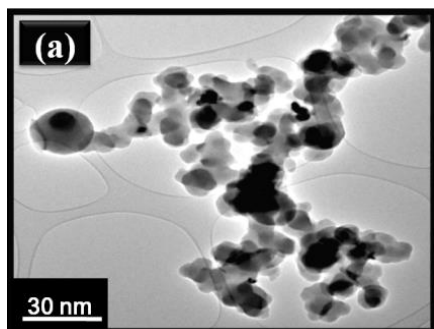


Fig 5 (b): TEM image of P-3

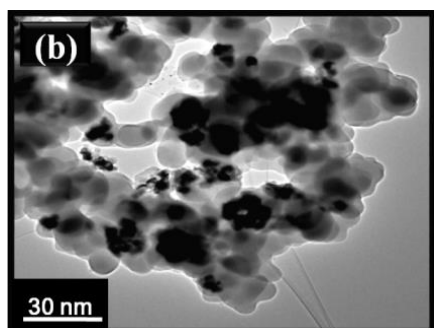


Fig 5 (c): TEM image of P-5

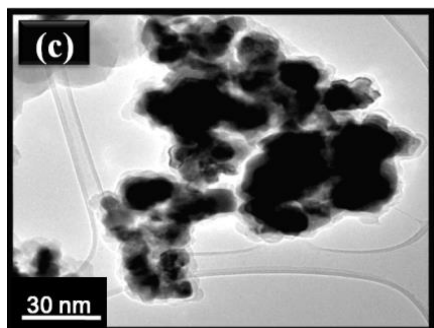


Fig 6: Variation in ϵ' as a function of frequency for (a) PPy (b) P-1 (c) P-2(d) P-3 (e) P-4 (f) P-5

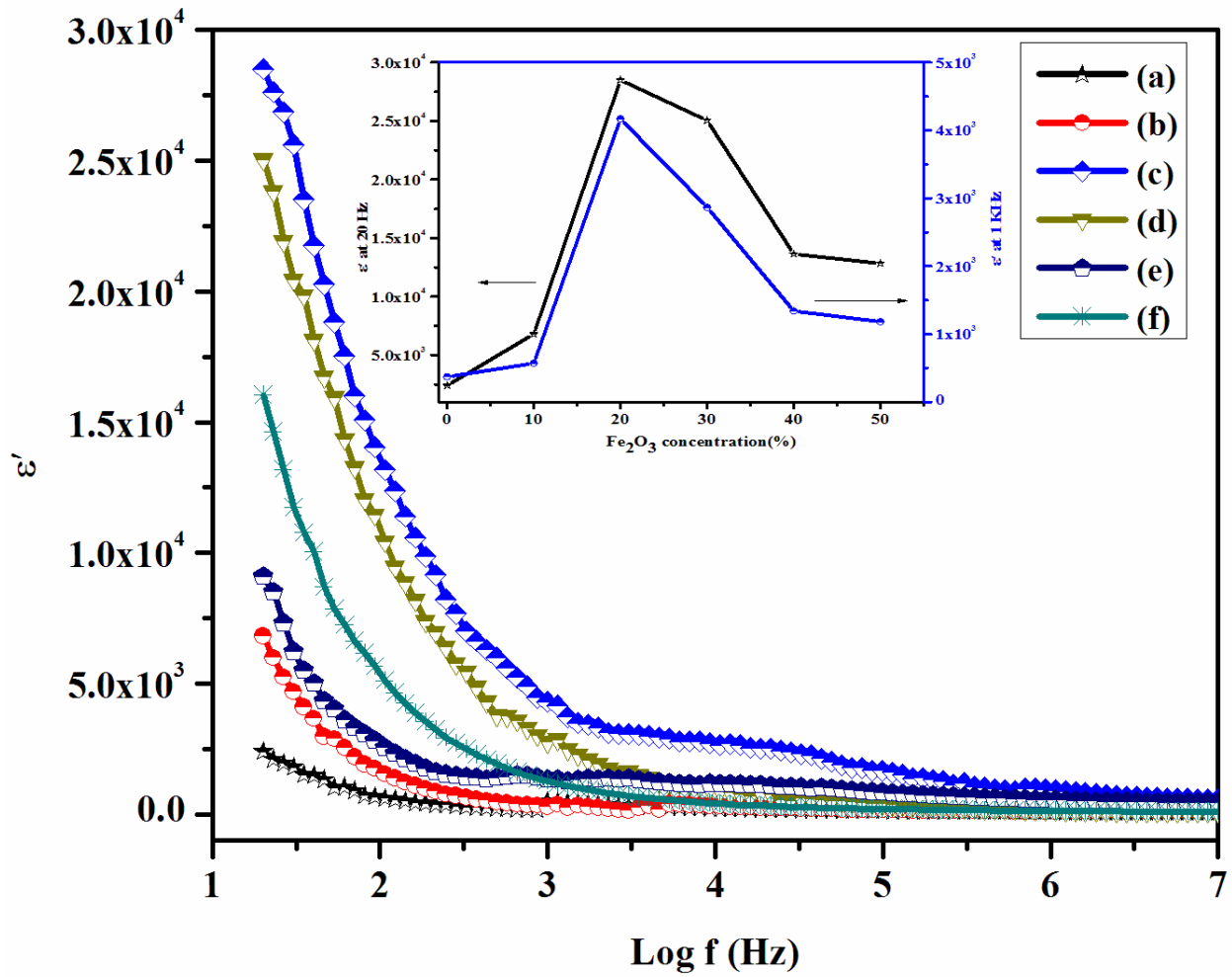


Fig 7: Variation in ϵ'' as a function of frequency for (a) PPy (b) P-1 (c) P-2(d) P-3 (e) P-4 (f) P-5

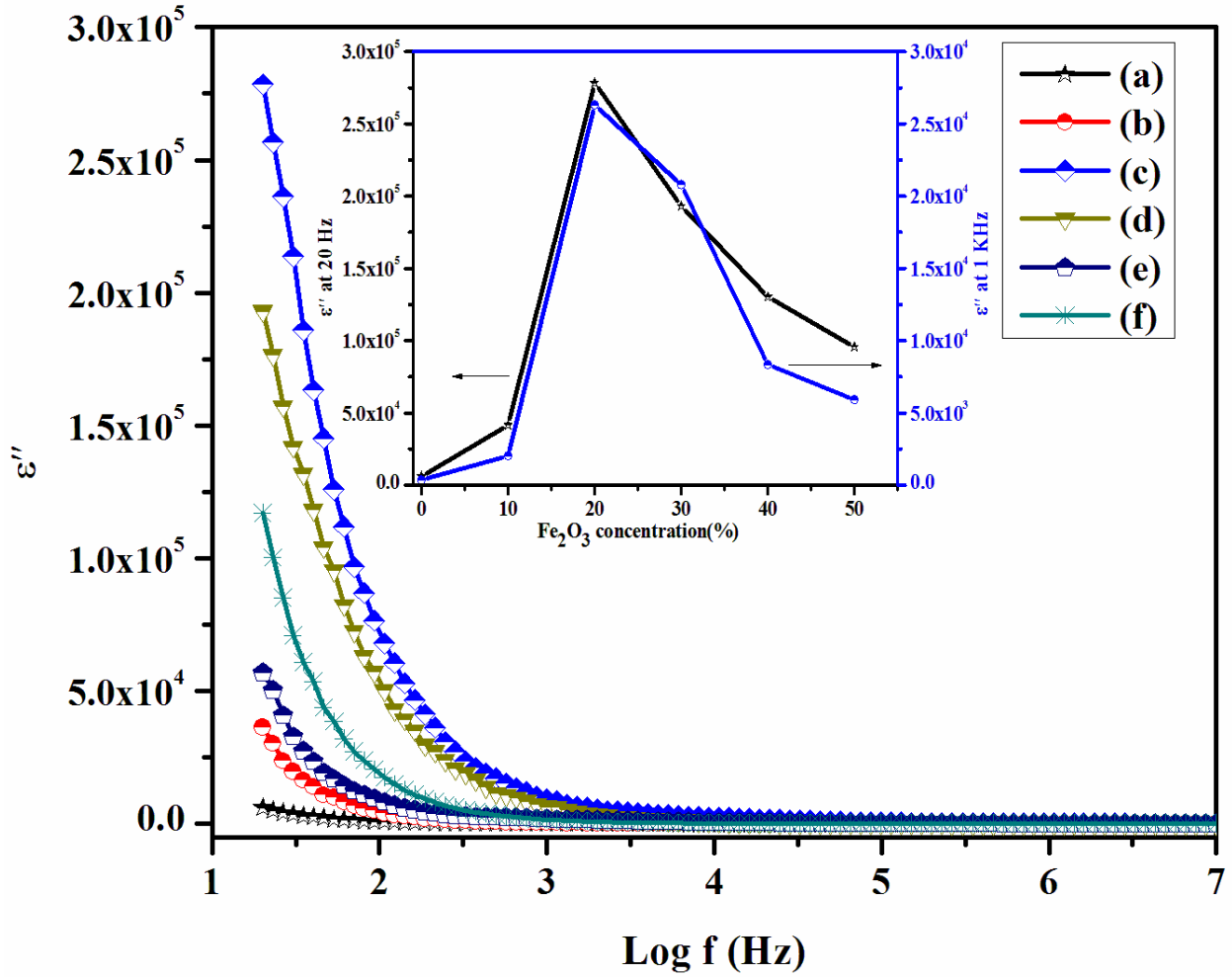


Fig 8: Variation in $\tan \delta$ for (a) PPy (b) P-1 (c) P-2(d) P-3 (e) P-4 (f) P-5

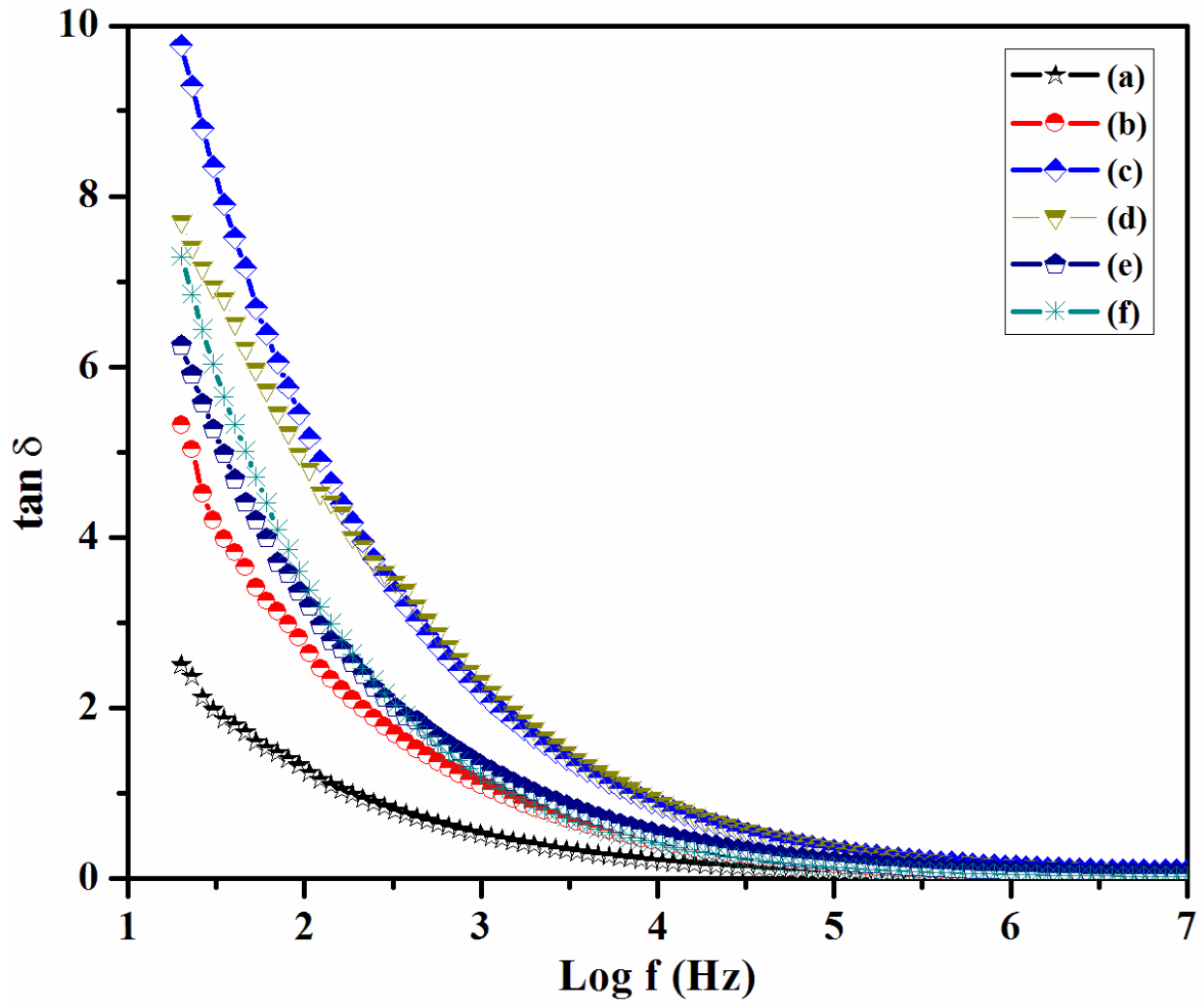


Table 1: Structural parameters for Fe₂O₃ and PPy-Fe₂O₃ nanocomposites

Sample	2θ (Degrees)	d-Spacing (Å)	β (Radians)	Cos θ (Degrees)	Thickness (nm)
Fe ₂ O ₃	33.177	2.699	0.0804	0.958	18
P-1	33.400	2.682	0.0402	0.958	36
P-2	33.400	2.682	0.0425	0.958	34
P-3	33.540	2.671	0.0425	0.958	34
P-4	33.800	2.651	0.0452	0.958	32
P-5	33.440	2.679	0.0482	0.957	30

Table 2: Fe₂O₃ loading effect on dielectric properties of PPy- Fe₂O₃ nanocomposites

Sample	Dielectric Constant at:		Dielectric Loss at:	
	20 Hz	1 KHz	20 Hz	1 KHz
PPy	2408	371	6032	361
P-1	6814	570	41593	2030
P-2	28500	4169	278472	26315
P-3	25048	2865	193104	20789
P-4	13632	1340	130349	8359
P-5	12848	1183	95633	5923